Article

Ultra-Sensitive Imaging and Interfacial Analysis of Patterned Hydrophilic SAM Surfaces Using Energy Dissipation Chemical Force Microscopy

Paul D. Ashby, and Charles M. Lieber

J. Am. Chem. Soc., **2005**, 127 (18), 6814-6818• DOI: 10.1021/ja0453127 • Publication Date (Web): 16 April 2005

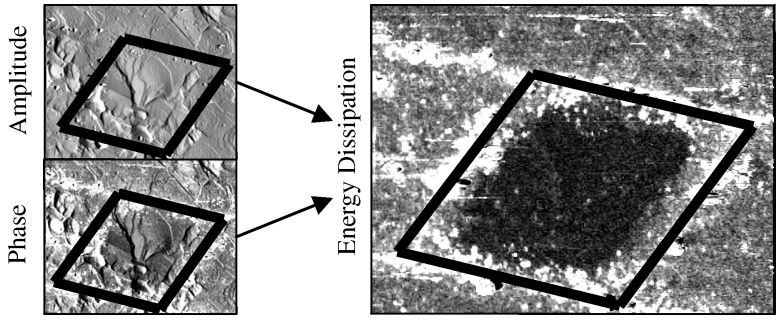

More About This Article

Additional resources and features associated with this article are available within the HTML version:

- Supporting Information
- Links to the 1 articles that cite this article, as of the time of this article download
- Access to high resolution figures
- Links to articles and content related to this article
- Copyright permission to reproduce figures and/or text from this article

View the Full Text HTML

J|A|C|S
ARTICLES
Published on Web 04/16/2005

Ultra-Sensitive Imaging and Interfacial Analysis of Patterned Hydrophilic SAM Surfaces Using Energy Dissipation Chemical Force Microscopy

Paul D. Ashby*,‡ and Charles M. Lieber

Contribution from the Department of Chemistry and Chemical Biology, Harvard University, Cambridge, Massachusetts 02138

Received August 3, 2004; E-mail: pashby@cmliris.harvard.edu

Abstract: Energy dissipation chemical force microscopy has been used to analyze the dissipative properties of chemically similar regions of hydroxyl- and carboxyl-terminated SAMs on gold with a hydroxyl-terminated tip. Energy dissipation imaging quantitatively isolates dissipative interfacial interactions from topography, producing a significantly more informative image than phase imaging. Also, energy dissipation force curves probed the rheological properties of the tip−sample interaction. Viscosity of the confined water increased slightly over that of the bulk, and SAM deformation was found to have a longer retardation time than restructuring of interfacial ions and solvent during tip−sample contact.

Introduction

Atomic force microscopy (AFM)[1] has revolutionized many fields of science as a result of its ability to image, manipulate, and characterize samples, from proteins to nanocrystals, with nanometer resolution.[2] The simple design of AFM provides the foundation for creative implementation of operating modes, such as friction force microscopy[3] or phase imaging to isolate particular tip−sample interactions. Its versatility is further demonstrated by its ability to refine tip−sample interactions using tips with specific physical[4] or chemical[5−7] properties. After its inception, phase imaging became extremely popular due to the high contrast for material properties. Subsequently, Cleveland and others elucidated the physical origin of the phase signal to be related to energy dissipation between the tip and sample.[8−11] However, there was no significant interest in measuring energy dissipation during tapping mode possibly because energy dissipation images generated thus far bear significant resemblance to the phase image with its strong topographical content.[10] Thus, researchers instead focused on understanding the phase signal in terms of energy dissipation.[7,12−15]

Concurrently, energy dissipation and damping have been of great interest in the fields of nanoindentation and nanorheology for determining the viscoelastic properties of materials. Quasistatic and dynamic[16] indentation measurements have been used to measure elastic modulus components[17] and adhesive forces[18] while rastering the sample to form an image. These indentation techniques apply high loads and cause significant deformation in the process of probing bulk properties. As a result, they are not suitable for less robust samples and the probing of interfacial interactions. Conversely, delicate water solvent structure was probed to obtain stiffness and damping information using subangstrom amplitudes.[19] However, subangstrom amplitudes make safe imaging of samples with topography challenging. Energy dissipation measurements that have sufficient amplitude to allow safe imaging, yet are gentle enough to probe interfacial interactions, are required to probe most biological and interfacial properties.

In this paper, we use energy dissipation chemical force microscopy for isolating and characterizing dissipative interactions with the AFM using tapping mode. Specifically, we imaged a patterned surface of hydroxyl- and carboxyl-terminated self-assembled monolayers (SAM) using a hydroxyl-terminated SAM tip in solution. By focusing on energy dissipation, the image is more sensitive than phase imaging for chemical

‡ Current address: Molecular Foundry, Lawrence Berkeley National Lab, Berkeley, CA 94720.

(1) Binnig, G.; Quate, C. F.; Gerber, C. *Phys. Rev. Lett.* **1986**, *56*, 930−933.
(2) Colton, R. J. *J. Vac. Sci. Technol., B* **2004**, *22*, 1609−1635.
(3) Meyer, G.; Amer, N. M. *Appl. Phys. Lett.* **1990**, *57*, 2089−2091.
(4) Martin, Y.; Wickramsinghe, H. K. *Appl. Phys. Lett.* **1987**, *50*, 1455−1457.
(5) Frisbie, C. D.; Rozsnyai, L. F.; Noy, A.; Wrighton, M. S.; Lieber, C. M. *Science* **1994**, *265*, 2071−2074.
(6) Noy, A.; Vezenov, D. V.; Lieber, C. M. *Annu. Rev. Mater. Sci.* **1997**, *27*, 381−421.
(7) Noy, A.; Sanders, C. H.; Vezenov, D. V.; Wong, S. S.; Lieber, C. M. *Langmuir* **1998**, *14*, 1508−1511.
(8) Cleveland, J. P.; Anczykowski, B.; Schmid, A. E.; Elings, V. B. *Appl. Phys. Lett.* **1998**, *72*, 2613−2615.
(9) Tamayo, J.; Garcia, R. *Appl. Phys. Lett.* **1998**, *73*, 2926−2928.
(10) Anczykowski, B.; Gotsmann, B.; Fuchs, H.; Cleveland, J. P.; Elings, V. B. *Appl. Surf. Sci.* **1999**, *140*, 376−382.
(11) Tamayo, J. *Appl. Phys. Lett.* **1999**, *75*, 3569−3571.
(12) Bhushan, B.; Qi, J. *Nanotechnology* **2003**, *14*, 886−895.
(13) Stark, M.; Moller, C.; Muller, D. J.; Guckenberger, R. *Biophys. J.* **2001**, *80*, 3009−3018.
(14) Wang, Y.; Song, R.; Li, Y. S.; Shen, J. S. *Surf. Sci.* **2003**, *530*, 136−148.
(15) Some researchers have directly measured energy dissipation using force modulation techniques in UHV (Holscher, H.; Gotsmann, B.; Schirmeisen, A. *Phys. Rev. B* **2003**, *68*. Hoffmann, P. M.; Jeffery, S.; Pethica, J. B.; Ozer, H. O.; Oral, A. *Phys. Rev. Lett.* **2001**, *87*, 265502. Gotsmann, B.; Fuchs, H. *Phys. Rev. Lett.* **2001**, *86*, 2597−2600).
(16) Burnham, N. A.; Kulik, A. J.; Gremaud, G.; Gallo, P. J.; Oulevey, F. *J. Vac. Sci. Technol., B* **1996**, *14*, 794−799.
(17) Asif, S. A. S.; Wahl, K. J.; Colton, R. J.; Warren, O. L. *J. Appl. Phys.* **2001**, *90*, 1192−1200.
(18) Tsukruk, V. V.; Huang, Z. *Polymer* **2000**, *41*, 5541−5545.
(19) Jeffery, S.; Hoffmann, P. M.; Pethica, J. B.; Ramanujan, C.; Ozer, H. O.; Oral, A. *Phys. Rev. B* **2004**, *70*, 054114-1-8.

10.1021/ja0453127 CCC: $30.25

contrast, and the chemical features are not obscured by surface topography while safely imaging rough surface topography. Subsequently, force curves are used to investigate the loss mechanisms revealed in the energy dissipation image.

Experimental Section

Theory. The equation for energy dissipation chemical force microscopy is derived from the equations describing stable oscillation dynamics of AFM cantilevers. Cleveland and others pioneered this effort by developing a model of cantilever dynamics based on time-averaged power balance, where the energy input into the cantilever by the tapping mode drive is dissipated by viscous drag and tip−sample interactions, $\overline{P_{in}} = \overline{P_{drag}} + \overline{P_{tip}}$.[8,11] The power of the first two terms is calculated by multiplying the cantilever velocity by the force applied to the cantilever and integrating over a single oscillation to obtain equations dependent on the tapping mode signals. The power dissipated by the tip−sample interaction is the difference between the input and drag powers. This is described by the equation

$$\overline{P_{tip}} = \frac{\pi k f^2}{f_0}\left[A_1 A_{1free}\left(\left(\frac{f_0}{f} - \frac{f}{f_0}\right)^2 + \frac{1}{Q^2}\right)^{1/2} \sin(\varphi) - \frac{1}{Q}\sum_{n\geq 1} n^2 A_n^2\right] \quad (1)$$

where the cantilever parameters, k, f_0, and Q, are the spring constant, resonant frequency, and quality factor, respectively; f is the tapping frequency; φ is the phase signal, and A_n are the amplitudes of the n harmonics of cantilever oscillation. Inclusion of the higher harmonics assumes a periodic but not sinusoidal wave form. The subscript "free" denotes the amplitude of the oscillation with no tip−sample interaction, such that A_{1free} is the term commonly designated A_0 in AFM literature. A thorough derivation of the energy dissipation equation is provided in the Supporting Information.

Sample Preparation. Magnetic AFM cantilevers were prepared by gluing small chunks of samarium cobalt on the backside of FESP cantilevers (Digital Instruments) using previously described methods.[20] Chromium and gold films were deposited on the tip apex using a thermal evaporator, and the tips were immersed in 1 mM 11-mercapto-1-undecanol (Aldrich) to form a self-assembled monolayer (SAM).[21] Flat gold surfaces were prepared by evaporating gold onto freshly cleaved mica and annealing. The surfaces were either placed directly into alkane thiol solution or patterned using soft lithography techniques.[22] The patterned SAM surfaces contained squares of 16-mercaptohexadecanoic acid (carboxyl SAM) surrounded by 11-mercapto-1-undecanol (hydroxyl SAM).

Data Collection. After adequate time for SAM formation, the tips and surfaces were rinsed with ethanol, blown dry with ultrapure nitrogen, placed in the instrument with 10 mM phosphate buffer (pH 2), and allowed to equilibrate. A multimode AFM (Digital Instruments), equipped with an E scanner and modified to achieve a 36 fm/$\sqrt{Hz}$ baseline noise at tapping frequencies,[23] was used during data collection. Cantilever oscillations were induced directly using magnetic fields from a small electromagnet located beneath the sample to avoid the complication caused by coupling the cantilever to acoustic modes in the solution. Similarly, magnetic drive simplified implementation of Q-control. Q-control is a method for modulating the effective cantilever damping using electronic feedback between the cantilever response and tapping piezo.[24,25]

For imaging, phase and amplitude data from a lock-in amplifier (SR830, Stanford Research) were recorded by extra analogue inputs on the Nanoscope IIIa controller. At the end of each image, the tip was raised off the surface in order to record the free tapping amplitude, A_{1free}, and phase, φ.

Contact mode force curves were collected using typical force curve techniques in force calibration mode. Tapping mode force curves were collected by recording a time course of the deflection signal and numerically converting to amplitude and phase signals. The time courses were sampled with 16-bit resolution at 1 MHz by a high-speed DAQ card using Labview, as the sample advanced and retracted from the tapping cantilever. The large bandwidth was necessary to measure higher harmonics of the cantilever motion for accurate calculation of the energy dissipation. Force curves using multiple tapping amplitudes and Q values were recorded.

Thermal noise data near the surface were recorded for calculation of the cantilever parameters, k, f_0, and Q. Force curves in hard contact with the surface were collected at the conclusion of each experiment to determine the sensitivity of the detector.

Data Analysis. All data analyses were performed using Igor Pro (version 4, Wavemetrics). Cantilever parameters were calculated by fitting the power spectrum of the deflection time course with the transfer function of a simple harmonic oscillator.[26] Amplitude and phase image data were scaled, and a 3 × 3 Gaussian matrix filter was applied to suppress uninformative high frequency noise. Subsequently, the energy dissipation was calculated from the cantilever parameters, frequency, amplitude, and phase data in the image. Only one lock-in amplifier was used during image collection such that the fundamental oscillation was the only harmonic available for the calculation. From experience with higher harmonics during force curves, the error due to only using the fundamental is approximately a 10% overestimation at this amplitude and Q.

Contact mode force curves were loaded and scaled for force as a function of Z-piezo displacement. They were subsequently offset to zero force in the region without tip−sample interaction and interpolated to be a function of tip−sample distance. Last, an offset in the tip−sample distance axis was added to overlap the curves in the contact region before averaging them together.

Energy dissipation force curve analysis began with recalculating the cantilever parameters for each Q value used during data collection, as the Q-control circuit can offset the resonant frequency if the phase delay is not exactly 90°. The tapping time courses were subsequently scaled for deflection, and the region with no tip−sample interaction was fit to calculate the tapping frequency accurately. The amplitude of the harmonics and phase of the fundamental were calculated using numerical techniques. Energy dissipation force curves were then computed, where five higher harmonics were adequate for convergence. Numerous energy dissipation time courses were interpolated to be a function of tapping amplitude and then averaged together.

Fine details of the experimental techniques are provided in the Supporting Information.

Results and Discussion

Energy Dissipation Imaging. Images of a patterned self-assembled monolayer surface on annealed gold are shown in Figure 1. The pattern consists of a square of carboxyl-terminated SAM, marked by thick black lines, surrounded by hydroxyl-terminated SAM. The low pH solution protonates the carboxyl groups and makes the two regions chemically similar so that both have long-range attractive interactions with the hydroxyl-terminated SAM surface on the tip. Oscillation amplitude is shown in frame a, with a free oscillation amplitude, A_{1free}, of 3.3 nm and a feedback setpoint value of 2.6 nm. Relatively small

(20) Ashby, P. D.; Chen, L. W.; Lieber, C. M. *J. Am. Chem. Soc.* **2000**, *122*, 9467−9472.
(21) Bain, C. D.; Troughton, E. B.; Tao, Y. T.; Evall, J.; Whitesides, G. M.; Nuzzo, R. G. *J. Am. Chem. Soc.* **1989**, *111*, 321−335.
(22) Xia, Y. N.; Whitesides, G. M. *Annu. Rev. Mater. Sci.* **1998**, *28*, 153−184.
(23) Ashby, P. D. Ph.D. Thesis, Harvard University, Cambridge, MA, 2003.
(24) Tamayo, J.; Humphris, A. D. L.; Miles, M. J. *Appl. Phys. Lett.* **2000**, *77*, 582−584.
(25) Tamayo, J.; Humphris, A. D. L.; Owen, R. J.; Miles, M. J. *Biophys. J.* **2001**, *81*, 526−537.
(26) Hutter, J. L.; Bechhoefer, J. *Rev. Sci. Instrum.* **1993**, *64*, 1868−1873.

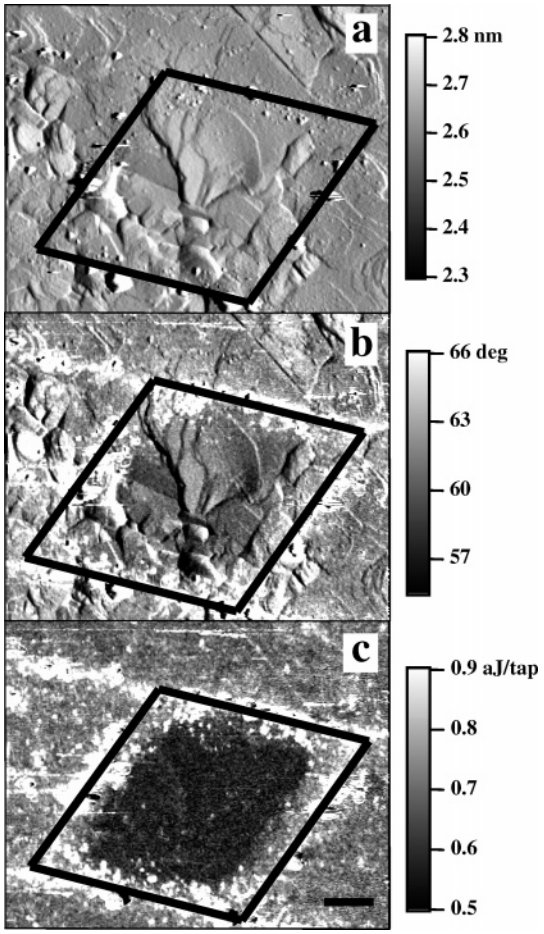

Figure 1. (a) Amplitude, (b) phase lag, and (c) energy dissipation images of a patterned SAM surface of hydroxyl surrounding a carboxyl square. The black square highlights the edges of the pattern. The topography is coupled into the amplitude and phase but compensated in the energy dissipation. The scale bar at the lower right is 200 nm.

amplitude was used to reduce the energy of the cantilever oscillation such that interfacial interactions can be measured. The annealed gold used is relatively flat with an root mean square surface roughness of 9 Å/μm^2 (height image not shown), but step edges and faults are still clearly visible in the amplitude image as topography modulates the tapping amplitude due to the finite bandwidth of the feedback loop. The largest fault has a step height of 2.3 nm, which shows up as a dark rift in the middle of the carboxyl square.

Power balance techniques were originally developed to understand the properties of the phase signal. By solving for phase from the energy dissipation equation, it is clear that the phase signal is a function of both amplitude and energy dissipation. The equation for phase, while assuming the tapping frequency is at resonance and the higher harmonics do not contribute, is

$$\varphi_1 = \sin^{-1}\left(\frac{Q\overline{P_{\text{tip}}}}{A_1 A_{1\text{free}}\pi k f} + \frac{A_1}{A_{1\text{free}}}\right) \qquad (2)$$

If the amplitude were fixed, the phase signal would be a function of the energy dissipation only and interpretation would be simpler. Unfortunately, this assumption is invalid, and the amplitude changes continuously as the AFM tip encounters surface topography. Thus, changes in amplitude couple to the phase signal, obscuring energy dissipation information, as shown in Figure 1b. The energy dissipation information in the phase image reveals itself through a slight darkening of the carboxyl SAM region and also as light stripes from contaminates deposited by the stamp around the outside of the carboxyl SAM region and extending out from the edges. Calculation of the energy dissipation image from eq 1 and the cantilever parameters, $k = 1.9_6$ N/m, $f_0 = 10.8_2$ kHz, and $Q = 7.1$, and tapping frequency, 10.704 kHz, produced the image shown in frame c. The topography, which is very evident in the phase image, is imperceptible in the energy dissipation image, including the large fault in the middle of the carboxyl region. This significantly increases the signal-to-noise ratio. The signal-to-noise ratio was calculated from the average values and standard deviation of the data within a rhombus with 0.5 μm long edges that are parallel to the black lines in Figure 1 for the carboxyl data and two triangular regions in the upper and lower right of the image for the hydroxyl region. Energy dissipation is 0.71 and 0.58 aJ per tap in the hydroxyl and carboxyl regions, respectively, with an error of 0.02 aJ per tap, leading to a signal-to-noise ratio of 6.6. The phase signal-to-noise ratio for the same regions was 0.94 such that the increased sensitivity for energy dissipation imaging was 7 times or almost an order of magnitude for this system. Moreover, the signal-to-noise ratio becomes greater for surfaces that are rougher, where more topography couples to the phase signal by inadequate feedback response. Thus, direct computation of the energy dissipation signal highlights interesting tip−sample interactions from the topography in the phase signal.

For complete isolation of energy dissipation information from topography, care is required to determine cantilever parameters, Q and f_0, and the phase offset properly. Previous derivations of energy dissipation formulas assumed that the tapping frequency is at resonance while most users tap with a frequency slightly lower than the maximum amplitude of the transfer function for stable feedback during imaging. Furthermore, tapping in solution at low Q causes the maximum of the transfer function to be intrinsically lower than the resonant frequency. Tapping off resonance causes the phase lag, when there is no tip−sample interaction, to deviate from 90°. Similarly, the free amplitude is a function of frequency, and nonresonant tapping causes miscalculation of the input power. Unfortunately, assuming that one is tapping at resonance and offsetting the phase to 90° causes the energy dissipation image to have zero dissipation when there is no tip−sample interaction, as expected, but the inaccuracy causes ineffective isolation of the energy dissipation from the topography once the cantilever dynamics are modulated by tip−sample forces. This causes the energy dissipation signal to resemble the phase signal more closely than the true dissipation. Fortunately, accurate determination of Q and f_0 from the noise power spectral density is simple. Similarly, inaccuracies in determining the deflection sensitivity, which is the largest source of error in determining the spring constant and tapping amplitudes, fortuitously cancel in the energy dissipation equation. Thus, accurate calculation of Q, f_0, and f is required to isolate best energy dissipation information for observing subtle changes in physical, chemical, or biological properties.

Conversely, users interested in observing subtle changes in topography should use the amplitude signal. For example, consider the idealized example where there is no energy

dissipation, the frequency is on resonance, and the Q is high enough that drag contributions from higher harmonics are negligible, then for small phase angle changes, eq 1 simplifies to

$$\varphi_1 \approx \frac{A_1}{A_{1\text{free}}} \tag{3}$$

The phase noise from the lock-in amplifier is the amplitude noise divided by the amplitude, so the amplitude signal-to-noise is related to the phase signal-to-noise by

$$\text{SNR}_\text{A} \equiv \frac{A_1}{N_\text{A}} = \frac{A_1}{A_1 N_\varphi} \approx \frac{A_{1\text{free}}\varphi_1}{A_1 N_\varphi} = \frac{A_{1\text{free}}}{A_1}\text{SNR}_\varphi \tag{4}$$

where N_φ and N_A are the phase and amplitude noise, respectively. Equation 4 shows that the signal-to-noise ratio for the amplitude is higher than the signal-to-noise ratio for the phase signal. Moreover, this effect is exaggerated when real imaging conditions are used, where $\sin(\varphi) \neq \varphi$ and the feedback loop squeezes the amplitude noise into the phase channel.[23] Using the amplitude channel to observe topography contrast and an energy dissipation channel to inspect interesting dissipative tip−sample interactions is optimal.

Most importantly, energy dissipation imaging lends itself to a more physical interpretation of the phenomena observed during the experiment than phase imaging. The information is quantitative, providing an absolute measure of the energy lost during the tip−sample interaction. These losses can be directly related to molecular processes at the apex of the tip, such as confinement and squeezing of a fluid, viscous deformation of a monolayer film, or forced unbinding of protein−ligand complexes. Inconsistency in probe geometry may cause significant variability of the results due to the differing contact area. Similarly, poorly defined surface chemistry reduces the knowledge about the true interfacial interactions being measured. Some variability is inherent in using nanoscale probes, yet it can be mitigated. For chemical force microscopy using thiol SAMs, we have found that the tip radius is often determined by a single gold grain with reproducible radius, and that the tip chemistry is consistent. Being very careful to avoid forces over 5 nN keeps the tip geometry intact and protects the SAM from being displaced. Other challenges to interpreting the dissipation may be that the losses are not homogeneous over the whole oscillation cycle or that the dissipation is a function of cantilever oscillation dynamics, but quantitatively recording dissipation marks a significant improvement over phase imaging. Thus, energy dissipation imaging is a powerful technique for imaging changes in molecular and interfacial properties sensitively.

Energy Dissipation Force Curves. Force curves aide the elucidation of viscoelastic interfacial phenomena occurring during energy dissipation chemical force microscopy. Previously, researchers performed contact mode force curves and related the hysteresis between the advancing and receding curves to the energy dissipated during each tap.[9] This method produced surprisingly consistent results, considering that the interaction velocity between the two measurements differed by 4 orders of magnitude. High precision contact mode force profiles between a hydroxyl-terminated SAM tip and hydroxyl- or carboxyl-terminated SAM surfaces similar to those used for the image above are displayed in Figure 2. Advancing and receding traces

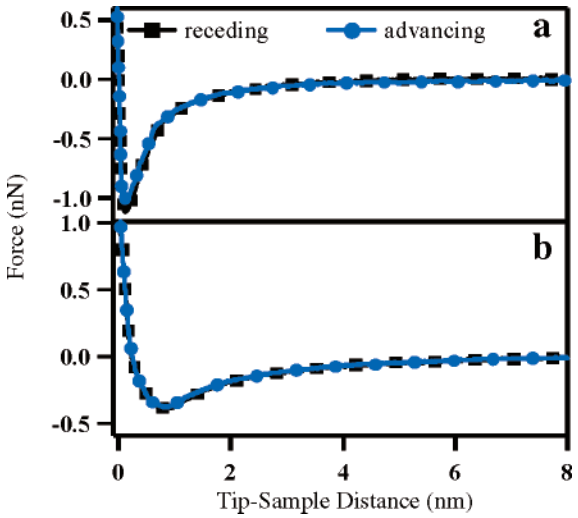

Figure 2. Advancing (blue circles) and receding (black squares) contact mode force curves for (a) hydroxyl- and (b) carboxyl-terminated surfaces show no hysteresis or energy dissipation.

showed no hysteresis, indicating that there is no energy dissipation during the cycling process and that the experiments were performed at quasi-equilibrium. Thus, the material relaxation time is likely to be much shorter than the 1 s time of the measurements.

Although both surfaces are chemically similar, their force profiles reveal significant differences. The attractive forces decay much faster for hydroxyl-terminated surfaces than for carboxyl surfaces, as shown in frames a and b, respectively. The different decay rate is most probably due to effects of functional group dissimilarity on hydration forces.[27] Repulsive forces in the contact region are similarly affected by the solvation. In these experiments, the contact between hydroxyl-terminated SAM surfaces is stiffer than can be accurately measured with the AFM, while the compliance of the carboxyl-terminated surface extends 1 nm into the surface from the point of maximum attractive force to an applied load of 1 nN. Stiff contact between the hydroxyl-terminated SAM surfaces could result from direct contact of the SAM headgroups after expulsion of all interfacial water. Conversely, the softer contact region for the carboxyl-terminated SAM surface would not be from direct SAM contact but instead from compression and restriction of the motion of bound solvated ions[28,29] near the "ionic" carboxyl groups, which are expected to be more compliant, and this is consistent with previous SFA experiments.[30,31]

Energy dissipation force curves, showing dissipation as a function of amplitude, are shown in Figure 3. Since attractive regime and repulsive regime tapping are distinctly different tip−sample interactions and since they sometimes share the same amplitude, the attractive regime data were separated from the repulsive regime data and subsequently plotted together. The differences are most noticeable in frames c and d, where the cantilever dynamics stay in the attractive regime over a large range of amplitude values. After the transition to repulsive tapping, the energy dissipation is significantly greater and

(27) Cappella, B.; Dietler, G. *Surf. Sci. Rep.* **1999**, *34*, 1−104.
(28) Marcelja, S. *Nature* **1997**, *385*, 689−690.
(29) Israelachvili, J.; Wennerstrom, H. *Nature* **1996**, *379*, 219−225.
(30) Colic, M.; Franks, G. V.; Fisher, M. L.; Lange, F. F. *Langmuir* **1997**, *13*, 3129−3135.
(31) Pashley, R. M. *Adv. Colloid Interface Sci.* **1982**, *16*, 57−62.

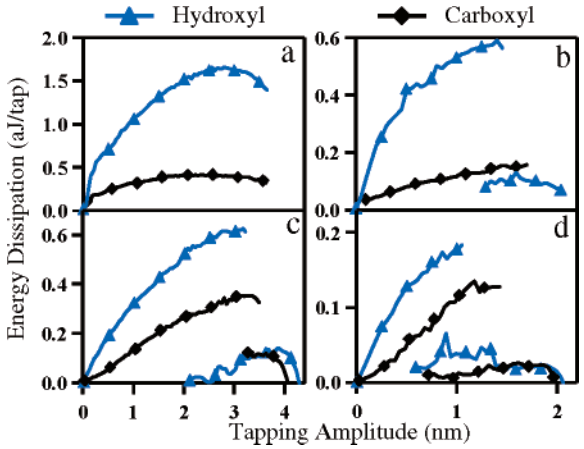

Figure 3. Energy dissipation force curves for SAM surfaces terminated with hydroxyl (blue triangles) and carboxyl (black diamonds). Curves were collected with $Q = 6.6$ (a, b) and $Q \sim 30$ (c, d), and free tapping amplitudes of 4 nm (a, c) and 2 nm (b, d).[32]

subsequently wanes as the amplitude is further reduced by surface impingement.

Tapping in the attractive regime, where tip−sample interaction forces are dominated by van der Waals and hydration forces, causes little energy dissipation relative to the repulsive regime for both the hydroxyl- and carboxyl-terminated SAM surfaces (Figure 3c and d). The dissipation increases before the tip−sample interaction reduces the amplitude, but diminishes as the amplitude is reduced. The increased dissipation implies that the confined solvent may have slightly increased damping, compared to that of the bulk. Recent AFM[19] and SFA[33] studies have similarly observed increases in damping for confined water. Reduction of the energy dissipation could be due to the smaller amplitude reducing the tip velocity and the extra dissipation associated with confined water.

In the repulsive regime, energy dissipation is significantly higher as the tip samples the contact region, which leads to a greater difference between the hydroxyl- and carboxyl-terminated SAM surfaces. With each tap, the tip causes viscoelastic deformation of the interfacial solvent and SAM structure. The contact mode force curves imply that the hydroxyl surface is readily dehydrated so that repulsive contact likely results in SAM deformation. Conversely, strongly bound ions near the carboxyl surface are not displaced easily. Thus, the repulsive contact results in both ion reorganization and SAM deformation. Higher dissipation while tapping on the hydroxyl surface implies that SAM deformation is more viscous than reorganization of bound ions and solvent. Consequently, the retardation time for SAM deformation would be relatively longer.

Energy dissipation force curves provide insight into the rheological properties of the tip−sample interaction on fast time scales. These properties are important for interpreting energy dissipation images and understanding the nature of tip−sample interactions. Further insight can be gained by performing energy dissipation force curves at multiple frequencies or by performing small amplitude experiments where the force gradients are homogeneous over the whole oscillation. The latter yields rheological parameters more readily.[18]

Conclusions

Energy dissipation chemical force microscopy isolates dissipative interactions from topography, producing a significantly more sensitive method of surface characterization than phase imaging. Harnessing the capability of energy dissipation chemical force microscopy to isolate and analyze dissipative interactions will greatly advance interfacial analysis with the AFM by pushing imaging beyond qualitative statements describing contrast to quantitative measurements that are more readily able to be interpreted physically. We used energy dissipation imaging to differentiate the subtle differences between hydroxyl- and carboxyl-terminated regions in a patterned SAM, which were buried in the topography information during phase imaging. Moreover, EDCFM force curves yielded information about the mechanism of dissipation, first, revealing that interfacial solvent likely has a slightly higher viscosity than that of bulk solvent, and second, SAM deformation is probably a large component to tip−sample dissipation due to its longer retardation time relative to reorganization of bound ions and solvent.

Acknowledgment. We thank the Air Force Office of Scientific Research for its generous support of this work. We also thank Jason Cleveland and Julia Forman for stimulating discussions, and Liwei Chen for valuable feedback concerning the manuscript.

Supporting Information Available: Derivation of energy dissipation equations and experimental details (PDF). This material is available free of charge via the Internet at http://pubs.acs.org.

JA0453127

(32) A slight deviation from 90° for the phase shift of the Q-control circuit causes the resonant frequency to be modulated with the Q. The cantilever parameters for the curves in Figure 3 are: carboxyl low Q ($k = 1.99$ N/m, $f_0 = 16.44$ kHz, $Q = 6.6$, $f = 16.236$ kHz), carboxyl high Q ($k = 1.99$ N/m, $f_0 = 16.52$ kHz, $Q = 32$, $f = 16.513$ kHz), hydroxyl low Q ($k = 1.99$ N/m, $f_0 = 16.53$ kHz, $Q = 6.6$, $f = 16.455$ kHz), and hydroxyl high Q ($k = 1.99$ N/m, $f_0 = 16.44$ kHz, $Q = 27$, $f = 16.489$ kHz).

(33) Zhu, Y. X.; Granick, S. *Phys. Rev. Lett.* **2001**, 8709.